Lawrence Berkeley National Laboratory
Recent Work

Title
A Wearable Microfluidic Sensing Patch for Dynamic Sweat Secretion Analysis.

Permalink
https://escholarship.org/uc/item/8k38r6h0

Journal
ACS sensors, 3(5)

ISSN
2379-3694

Authors
Nyein, Hnin Yin Yin
Tai, Li-Chia
Ngo, Quynh Phuong
et al.

Publication Date
2018-05-01

DOI
10.1021/acssensors.7b00961

Peer reviewed

A Wearable Sweat Sensing Patch for Dynamic Sweat Secretion Analysis

Hnin Yin Yin Nyein[1,2,3], Li-Chia Tai[1,2,3], Quynh Phuong Ngo[1,3], Minghan Chao[1], George Zhang[1,3], Wei Gao[1,2,3], Mallika Bariya[1,2,3], James Bullock[1,2,3], Hyungjin Kim[1,2,3], Hossain M. Fahad[1,2], Ali Javey[1,2,3]*

[1]Department of Electrical Engineering and Computer Sciences, University of California, Berkeley, California 94720, USA.

[2]Berkeley Sensor and Actuator Center, University of California, Berkeley, California 94720, USA.

[3]Materials Sciences Division, Lawrence Berkeley National Laboratory, Berkeley, California 94720, USA.

KEYWORDS Wearable biosensors, Microfluidic device, Sweat patch, Multiplexed sensing, Electrochemical sensor, Flexible electronics

ABSTRACT Wearable sweat sensing is a rapidly rising research driven by its promising potential in health, fitness and diagnostic applications. Despite the growing field, major challenges in relation to sweat metrics remain to be addressed. These challenges include sweat rate monitoring for its complex relation with sweat compositions and sweat sampling for sweat dynamics studies. In this work, we present a flexible microfluidic sweat sensing patch

that enhances real-time electrochemical sensing and sweat rate analysis via sweat sampling. The device contains a spiral-patterned microfluidic component that is embedded with a Na^+-selective sensor and an electrical impedance-based sweat rate sensor on a flexible plastic substrate. The patch is enabled to autonomously perform sweat analysis by interfacing the sensing component with a printed circuit board that is capable of on-site signal conditioning, analysis and transmission. Progressive sweat flow in the microfluidic device, governed by the pressure induced by the secreted sweat, enhances sweat sampling and electrochemical detection via a defined sweat collection chamber and a directed sweat route. The characteristic of the sweat rate sensor is validated through a theoretical simulation, and the precision of the flow rate is verified with a commercial syringe pump and a Macroduct® sweat collector. Off-body and on-body simultaneous monitoring of Na^+ concentration and flow rate are also demonstrated for sensor functionalities. This sweat sensing patch provides an integrated platform for a comprehensive sweat secretion analysis and facilitates physiological and clinical investigations by closely monitoring interrelated sweat parameters.

The burgeoning field of wearable electronics technology provides a promising future for personalized health assessment.[1-9] While there is a prime development in wearable devices for monitoring physical activity and vital signs,[5,6,9-13] major effort is still needed to realize reliable wearable biosensors by decoding mutually dependent health metrics for personalized healthcare. Sweat, a popular target for wearable biosensors,[7,8,14-22] has been

shown as an increasingly important biofluid for health monitoring, disease diagnosis and athletic performance evaluation.[23-27] Over the past years, wearable sensors for sweat analysis have been demonstrated for detection of a wide range of sweat constituents, varying from small ions and metabolites to large hormones.[7,8,14-20,23,24] Despite these major efforts, a number of key elements related to sweat sensing are still needed to be addressed, specifically the role of sweat secretion rate and effective sweat sampling for enhanced dynamic sweat analysis.

Due to the complex nature of sweat secretion and reabsorption mechanism,[20,21,28] sweat composition concentrations and sweat rate are inextricably linked. For instance, sweat $[Na^+]$ and $[Cl^-]$ are more concentrated at higher sweat rates. Lactic acid, urea, and creatinine increases with decreasing sweat rate.[25,28,29] Beside, during prolonged exercise, continuance of a high sweat rate can lead to dehydration, which in turn leads to impaired athletic performance.[27] Despite the significance of sweat rate, current research development on wearable sensors cannot monitor sweat constituents along with sweat rate in a single platform. Traditionally, sweat rate measurements were conducted based on body mass change and sweat patch analysis.[27,30] These methods involve logistic complications and require trained personnel to perform experiments in specialized laboratories. Another method for local sweat rate measurement is capacitance hygrometry,[31,32] but this method requires careful calibration of the sensor for humidity variations in the environment. More recently, optical sweat rate

sensors have been developed,[33] but they cannot be utilized for continuous autonomous measurement.

Another major overlooked factor in wearable sweat sensing is sweat sampling. Appropriate sweat sampling is crucial to obviate measurement artifacts from evaporation and contamination of sweat specimens. Effective sweat transport through fast sampling can minimize the mixing and carry-over effect of the new and old sweat.[20] These undesirable effects can be overcome by utilizing microfluidics. Microfluidics facilitate continuous sampling by directing sweat along a controlled channel and enhance sensing in a well-defined encapsulated chamber. It decouples the sweat generation and sensing to eliminate external contamination while preventing sweat evaporation. At the present, only a few wearable sweat sensors have been demonstrated by employing microfluidic chamber for capturing and sampling sweat.[33,34]

Here we introduce a wearable sweat sensing patch that merges an electrochemical sensor and an electrical impedance-based sweat rate sensor inside a microfluidic channel for effective sweat secretion analysis. The system provides an important advance in sweat analysis by providing a mechanism to analyze sweat content in real-time by minimizing averaging effect overtime. It enables detection of sweat analytes, specifically Na^+, in a defined microfluidic reservoir and directs sweat flow to accurately quantify sweat secretion rate. While the Na^+ and sweat rate sensors individually provide information on physiologically relevant quantities, together they can

be utilized for a comprehensive study of the relation between sweat metrics, and the platform can be configured to other sweat biomarkers for investigation of sweat secretion mechanisms. To realize these capabilities, our system combines a conventional soft microfluidic platform with a flexible plastic substrate to achieve a conformal and robust sweat sensing patch for long-term continuous measurement (Figure 1). The sweat sensing patch facilitates efficient sweat sampling and enhances capturing of dynamic changes in sweat compositions by spontaneously pumping the secreted sweat along the microfluidic channel. The device also minimizes evaporation and contamination of sweat samples by harvesting sweat in a detection chamber. By integrating commercially available printed-circuit board (PCB) technology, we deliver a fully-integrated system that interfaces the sensor patch with a PCB for signal conditioning and data transmission to provide real-time feedback and inform users of their sweat behavior. The system can be expanded to a wide range of sweat biomarkers for detailed studies of the role of sweat in relation to physiological conditions.

RESULTS AND DISCUSSION

The flexible sweat sensing patch is comprised of two major components: a microfluidic electrochemical and electrical sensing component and a printed circuit board component. The sensing component contains four layers: a spiral-patterned microfluidic channel, two parallel Au spirals, a parylene-C insulation layer, and Na^+ sensing electrodes (Figure 1a).

The microfluidic channel is prepared with polydimentylsiloxane (PDMS) to have conformal contact with the skin, and each loop of the spirals is separated by 1 mm to minimize parasitic effect. The microfluidic has a 0.4-mm depth and a 5-mm diameter opening that acts as a sweat collection reservoir and a 0.5-mm outlet with a microchannel of 600 μm by 200 μm in width and depth, respectively. This channel can contain sweat volume up to 14 μL and can approximately last 50 min based on an average arm sweat secretion rate of 10 nL/min/gland.[21] The microfluidic channel is covalently bonded to polyethylene terephthalate (PET) containing sensing electrodes layer, via O_2 plasma etching and silanization[35] to enclose the microfluidic channel firmly.

Na^{+} sensing electrodes are 1-mm diameter and are located at the opening of the microfluidic device (Figure 1b) such that Na^{+} detection takes place as soon as sweat accumulates at the chamber. As sweat secretes and fills up the chamber, the initial sweat is transported along the channel while fresh sweat continuously replaces the old sweat. Here sweat transport along the microchannel is driven by the natural pressure due to perspiration and the capillary action. This mechanism allows the sensors to effectively capture the dynamic changes of the sweat contents. The impedance-based sweat rate sensor lies on top of the insulation layer which electrically isolates the metallic wires from the Na^{+} sensing electrodes. The sweat rate sensor contains two parallel Cr/Au spirals with a width of 150 μm and a separation of 100 μm. These spirals are aligned with the microfluidic channel. The

detailed fabrication processes are illustrated in Figure S1. Sweat rate is quantified by measuring the magnitude of the impedance between the two spirals. As sweat travels along the channel, the impedance magnitude drops with increasing sweat volume due to a decrease in the effective resistance and an increase in the capacitance. Thus, a relation between admittance magnitude (1/|impedance|) and the distance sweat traveled can be acquired. This relation then allows admittance magnitude to be converted into sweat volume contained in the channel within a constant time interval.

Figure 1c depicts a fully-integrated sweat patch worn on a user's wrist. We employed the capabilities of the PCB by bringing two detection modalities into a single unit to achieve simultaneous measurement and analysis of Na^+ concentration and sweat rate. Each path is electrically isolated to ensure no signal interference and to relay the correct signal output. The PCB is designed such that impedance path has 0.1 % resolution and the open circuit potential (OCP) path has 0.1 mV resolution. Figure S2 and S3 illustrate the schematics of the PCB layout for the impedance and the OCP measurement of the device, and detailed PCB design is described in the Experimental Section. The signal is conditioned and transmitted via Bluetooth and is displayed in a customized cell-phone app for easy read-out.

The electrical impedance-based sweat rate sensors (Figure 2a) were firstly characterized in a solution containing NaCl concentration of 15 and 60 mM, which are relevant to the physiological range of sweat Na^+ concentration.[21] Measurements were operated at an optimal frequency of

100 kHz such that the impedance measurement is dominated by the resistance. This minimizes the contribution from the parasitic capacitance due to the spiral arrangement. The experimental results of the change in admittance with distance fluid traveled in 15 and 60 mM NaCl solutions are plotted along with the simulation results in Figure 2b, which shows well-agreed polynomial trend between the experimental and the simulation results. As the resistance between two Au wires changes with the ionic strength of the solution, it is necessary to study the influence of this change on admittance. As shown in Figure 2b, admittance of the Au electrodes increases with increasing concentration which is due to increasing electrical conductivity at higher ionic concentration. To further explore the relation between the admittance, the distance of the fluid traveled, and the concentration of the NaCl solution, admittance changes depending on the latter two parameters were experimentally recorded in 15, 30, 60, and 120 mM NaCl solutions. The result is shown as a surface plot in Figure 2c. The admittance increases in polynomial behavior with respect to both increasing concentration and distance of the fluid traveled. This plot allows simple sweat rate conversion by finding the corresponding distance traveled at a measured admittance and Na^+ concentration. These characterization studies allow us to understand the electrical behavior that corresponds to a specific pattern, a spiral in this case, and hence it is possible to achieve the desired patterns with performance validation through simulation.

Sweat rate is expected to vary from 1 to 20 nL/min/gland. On the arm region, there are typically 150 glands/cm^2.[21] In this case, sweat rate is estimated to be as high as 2 µL/min for the 5-mm diameter sweat collection area. To ensure that the device accurately outputs the flow rate within this range, flow rate measurement computed from the sweat rate sensor is compared with the known pump rate from a commercial syringe pump meter. In Figure 2d, a constant concentration of 30 mM NaCl solution was flowed into the microfluidic channel at various flow rates ranging from 0.14 to 2.0 µL/min. The change in admittance with time was recorded. The measured admittance versus time does not increase linearly with time due to the non-linear relationship between the admittance and the distance that the fluid travels. The measured admittance values are converted to distance traveled using the relation obtained in Figure 2c to compute the flow rate. In Figure 2e, the results show that the relation between the measured microfluidic flow rate and the pump rate is proportional with a slope of 0.92. To enhance the accuracy of the sweat rate sensor, the flow rate can be easily corrected for the subsequent measurements by using this relation. The standard deviation at each pump rate is shown as an error bar at each point, and the error at each flow rate varies between 6 and 11 %. As evidenced from the experimental results, the sensor can accurately quantify the flow rate that is in the physiologically relevant range of the sweat rate.

Resistance of a metal changes with temperature, hence it is critical to measure the temperature dependence of the sensor. For this study,

admittance was measured in a constant 60 mM NaCl solution at the physiologically relevant skin temperature range.[36] Figure 2f demonstrates the experimental results obtained by heating up the sweat rate sensor from 25 to 33, and 39 °C. The results show that the change in admittance due to temperature variation is insignificant as the difference is approximately the same as the measurement variations between separate trials at a single temperature (Figure S4). The largest variation in admittance occurred at the longest distance traveled is only 3.6 %. Therefore, temperature influence on sweat rate measurement is negligible.

To function effectively, the sensor needs to simultaneously monitor the sodium concentration and sweat rate without influencing each other. Figure S5 shows typical performance of a Na^+ working electrode and a reference electrode. Sensor performance is typically measured in a still solution. When the test solution is in a constant motion, the detection signal may vary due to local changes in the net ionic concentration.[37] Therefore, a series of experiments were conducted to investigate the interplay between the $[Na^+]$ and sweat rate. In Figure 3a, a constant concentration of 30 mM NaCl solution is flowed at three different constant rates: 0.4, 1.4, and 2.8 µL/min. The measured admittance results are converted into flow rate at each measurement period, which is taken at every 5 s, and the result is indicated in Figure 3b. It shows that the OCP measured by the Na^+ sensor gives a relatively stable reading at different flow rates. Hence the fluid flow rate has minimal effect on the sensor detection signal. While Na^+ sensors show robust

performance at various flow rates, it is also crucial to ensure that the sweat rate sensor can accurately output flow rate with respect to varying NaCl concentration. Therefore, three different concentrations of NaCl solution was flowed into the device at a constant flow rate of 1 μL/min as shown in Figure 3c. The sensitivity of the Na^+ sensor was 56 mV/decade, and the measured flow rate variations were less than 5 % from the pump rate. Therefore, varying NaCl concentration has negligible influence on the flow rate measurement of the device. Lastly, the real-time response of the sensor to changes in flow rate at a constant NaCl concentration was studied. In Figure 3d, 30 mM NaCl solution was injected into the device at three different flow rates in a stepwise manner. Starting at flow rate as low as 0.08 μL/min, the flow rates measured based on the admittance and the OCP were recorded. At 140 s, the flow rate was increased to 0.75 μL/min and then to 3 μL/min. The sweat rate sensor shows very fast response to sudden changes in flow rate. Figure 3e depicts [Na^+] and flow rate measurements at a constant pump rate of 0.8 μL/min. When [Na^+] is changed from 15 to 60 mM, flow rate measurement remains relatively constant. These studies indicate that the sensor can accurately perform simultaneous measurement with minimal influence from each of the sensing path and hence lay a platform for contemporary sweat rate and electrochemical detection studies.

On-body performance of the sweat rate sensor was validated with the Macroduct® which is a standard sweat collection system used in cystic fibrosis diagnosis.[38] It is useful for optical sweat rate measurement since it

11

can be worn on a small region of the body to measure the local sweat contents and sweat rate. For this study, a Macroduct® and a sweat sensing patch were worn on each side of a subject's wrists. A subject wearing the sweat sensing patch is shown in Figure 4a. The subject cycled on an ergometer at a constant power load of 150 W and the optical images of the Macroduct® were taken every 3 to 4 min as soon as sweat began to flow into the Macroduct®. The sweat patch was packaged such that the PDMS interfaced with the skin and a medical tape was used to tightly wrap around the wrist to ensure the device is in conformal contact with the skin. Here sweat rate conversion was done based on Figure 2c as previously discussed. In Figure 4b, sweat flowed into the Macroduct® at 11 min after the start of the cycling, and the first optical sweat rate measurement was taken at 14 min. The microfluidic sweat patch began to respond at 13 min which was soon after the Macroduct® sweat collection began. Sweat rate gradually increased as exercise began and peaked between 26 min and 30 min. The sweat rate measurement obtained from the sweat patch shows consistent pattern with that from the Macroduct®. This result is also in agreement with previous studies on sweat rate analysis.[31,32] The discrepancy in absolute sweat rates arises from the difference in sweat collection area. The study shows that the microfluidic sweat rate sensor can be used for continuous measurement and can be as reliable as the optical sweat rate measurement from the Macroduct®.

Finally, the sweat patch was used for on-body simultaneous analysis of Na^+ and sweat rate to demonstrate its feasibility for continuous health monitoring applications. In this trial, subjects wore the sweat sensing patch on the wrists and performed stationary cycling at a constant load for nearly an hour. The trials were performed with a 5-minute ramp-up and a 45-minute biking at 150 W, followed by a 5-minute cool-down session as presented in Figure 4c and Figure S6. For subject 1 shown in Figure 4c, Na^+ sensor starts responding at 12 min after the trial begins, which is soon after sweat secretion starts and accumulates in the collection chamber. The $[Na^+]$ quickly rises to a peak concentration at 22 min, which is the time sweat rate measurement begins. Here the sweat rate sensor responds approximately 10 min after the Na^+ sensor because it takes some time to fill the sweat accumulation chamber before reaching the channel containing impedance-based sweat rate sensor. Based on an approximated average sweat rate of 0.4 μL/min, the reservoir is expected to be filled up in 20 min after perspiration begins. Therefore, the result is in agreement with the estimated time frame. An important behavior observed in this study is that the Na^+ and sweat rate sensors exhibit a similar trend. When $[Na^+]$ gradually increases at the initial stage of the trial, sweat rate also increases and reaches a relatively stable region similar to the $[Na^+]$. Near the end of the trial, both sweat rate and $[Na^+]$ decrease. This phenomenon can be explained by the fact that sweat rate and $[Na^+]$ have a proportional relationship.[28,29] On-body experiment of subject 2 shown in Figure S6 also shows similar behavior as

subject 1. At the end of the trial, when sweat rate reaches zero, [Na^{+}] reaches a relatively stable value. Sweat rate behavior in these trials are consistent with the previous result in Figure 4b and the literature.[31,32] The experimental results show that the sensor can be used to achieve more detailed study of sweat rate relation to sweat biomarkers. By characterizing both sweat rate and sweat biomarkers in temporal dimensions concurrently, our sweat sensing patch can assist a deeper understanding of the sweat secretion dynamics and allow thorough clinical studies of their roles in relation to health physiology.

CONCLUSION

We demonstrated a wearable sweat sensing patch based on a microfluidic detection system for efficient dynamic sweat secretion analysis of sweat Na^{+} concentration and sweat rate. The device greatly expands the biosensing platform by combining electrochemical and electrical sensing modalities on a single microfluidic platform. Integration of microfluidic channels and sensors fabricated on PET is demonstrated to provide reliable detection mechanism and measurement analysis. We also showed its capabilities for enhanced *in situ* measurement by performing on-body studies. System integration of OCP and impedance measurement tools in a single PCB facilitates simple analysis and easy read-out. This device addresses major challenges in wearable sweat sensing and facilitates dynamic sweat analysis by simultaneously monitoring interrelated sweat parameters. Future studies will focus to improve temporal resolution of the

sensors and to achieve easy and high-throughput fabrication. Detailed investigation of correlations between sweat rate and sweat biomarkers will be conducted for population-based physiological and clinical investigations. We envision that our sweat sensing patch can significantly advance the field of wearable biosensors and promote interdisciplinary collaborations toward realizing personalized medicine.

EXPERIMENTAL SECTION

Materials

(3-Aminopropyl)triethoxysilane (APTES), sodium ionophore X, bis(2-ethylehexyl) sebacate (DOS), sodium tetrakis [3,5-bis(trifluoromethyl)phenyl] borate (Na-TFPB), high-molecular-weight polyvinyl chloride (PVC), tetrahydrofuran, cyclohexanone, polyvinyl butyral resin BUTVAR B-98 (PVB), sodium chloride (NaCl), 3,4-ethylenedioxythiophene (EDOT), and poly(sodium 4-styrenesulfonate) (NaPSS) were purchased from Sigma Aldrich. The PDMS (Sylgard 184) was purchased from Ellsworth Adhesives. Moisture-resistant 100 μm-thick PET was purchased from McMaster-Carr (Los Angeles, CA).

Fabrication of the sensing component

Fabrication process of the microfluidic electrochemical sensors is illustrated in Figure S1. Briefly, PET was cleaned with acetone and IPA, followed by O_2 plasma etching at 90 W, 200 mtorr for 2 mins. The conductive sensing electrodes were patterned via photolithography using photoresist (Shipley Microposit S1818). A Cr/Au layer of 30/80 nm thickness was

thermally evaporated, followed by lift-off in acetone. A 600 nm Parylene-C insulation layer was then deposited using SCS Labcoter 2 Parylene Deposition System. The insulation layer was then etched with O_2 plasma for 1 min at 90 W to promote adhesion of the photoresist on parylene. The spiral-patterned electrodes were defined on top of the insulation layer by photolithography using LOR5A and S1818. Then 30/80 nm Cr/Au were deposited by thermal evaporation, followed by lift-off in PG remover. Furthermore, 1 mm-diameter electrochemical sensing circles were defined by photolithography, followed by thermal silver evaporation and lift-off in acetone. Lastly, one of the silver circle is etched with 8 M HNO_3 to expose the Au layer. The electrodes were then functionalized into Na^+-selective sensors using previously reported method.[7]

The microfluidic channel was fabricated using SU8 negative photoresist to achieve 200 μm thickness of channel depth. PDMS was then poured onto the SU8 mold to pattern the spiral-shaped microfluidic channel. To achieve permanent bonding between the PET and the PDMS, the PET with functionalized electrodes (the sensing layer) was etched in O_2 plasma for 1 min at 70 W and coated with aqueous 1 % (v/v) APTES for 20 mins. The layer was rinsed with water and dry. The microfluidic PDMS layer was treated with O_2 plasma for 1 min at 70 W then immediately bonded with the sensing layer and baked at 65 ℃ for 15 mins. The devices were left overnight before usage.

Development of the PCB

The printed circuit board is powered by a rechargeable lithium-ion battery with a nominal voltage of 3.7 V. The circuit diagram of the analog signal-conditioning block of the device is shown in Figure S2 and S3. The circuit has two functionalities: impedance and OCP measurement. For impedance measurement, AD5933, a high precision impedance converter, is used as the core. Here, the operating frequency is set to 100 kHz and the AC signal amplitude is set to 400 mV. Both input and output of AD5933 are biased to mid-rail to prevent any DC bias that can polarize the Au electrodes. The signal from the impedance is sampled by the on-chip analog-to-digital (ADC) converter, and a discrete Fourier transform (DFT) algorithm is used for impedance calculation. For the OCP measurement, a configuration similar to two-electrode potentiostat is used. For the reference electrode potential, a voltage buffer is utilized to provide a mid-rail reference voltage. The reference electrode connects to the negative input of the operational amplifier to limit the current flow to less than 0.1 pA. The working electrode connects to a voltage buffer and then to a fourth-order Sallen-Key low-pass filter with cut-off frequency of 0.88 Hz to eliminate high frequency noises. A 16-bit ADC (LTC1864) is used to measure the potential difference between working and reference electrodes. Both parts are controlled by a microcontroller Atmega328p, and the microcontroller sends data to Bluetooth module via UART protocol. The Bluetooth module wirelessly transmits the data to mobile phone interface for display.

Characterization and off-body analysis of the sweat rate sensor

Sweat rate sensors were characterized using solutions containing various NaCl concentrations. Flow rates experiments were carried out using Harvard Apparatus PHD 2000 Syringe Pump. The OCP measurements in off-body analyses were normalized to a set potential. Sweat rate measurement was filtered in Matlab to smooth data using a moving average filter.

Theoretical simulations of the sweat rate sensor

Impedance simulations were conducted using ANSYS HFSS' 3-D, full-wave finite element method (FEM) solver. The sensor was simulated at 100 kHz and 25 °C with various NaCl concentrations: 15 mM (σ = 0.175 S/m, $\varepsilon_r \approx$ 670) and 60 mM (σ = 0.615 S/m, $\varepsilon_r \approx$ 2700).[39-42]

On-body analysis of the microfluidic device

On-body human trials were carried out at the University of California, Berkeley in compliance with the human research protocol (CPHS 2014-08-6636) approved by the Berkeley Institutional Review Board (IRB). Two on-body trials were performed to evaluate the measurement accuracy of the sweat rate sensor in comparison with a Macroduct® sweat collector and to examine sensor performance as a whole. An electronically braked leg-cycle ergometer (Kettler E3 Upright Ergometer Exercise Bike) was used for stationary cycling trials. Subjects' wrists were wiped and cleaned with alcohol swab and gauze before placing the sensing patch. Cycling protocol included a 5-min ramp-up and a 30-45-min biking at a power of 150 W, followed by a 5-min cool-down session. Data were directly recorded in a mobile phone via a customized cellphone app. Sweat rate measurements

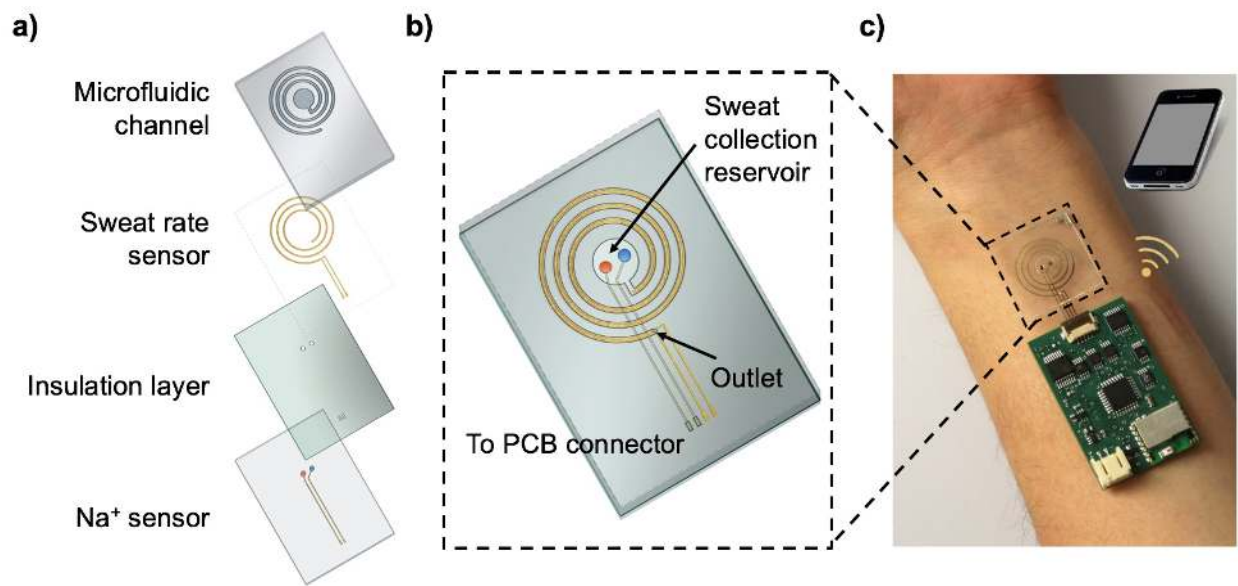were filtered using the same functions as in off-body analyses.

Figure 1. Schematics of a wearable sweat sensing patch. (a) The microfluidic sweat sensor is comprised of four layers: a spiral-patterned microfluidic channel, a pair of parallel Au electrodes for sweat rate sensing, a parylene-C insulation layer, and Na^+ sensing electrodes. (b) A stacked view of the microfluidic device. The spiral Au electrodes for sweat rate sensing are aligned with the microfluidic channel. The sodium sensor is located at the sweat collection reservoir. (c) The sweat sensing patch is conformal to the skin and can be comfortably worn on a user's wrist. The analyzed data can be wirelessly transmitted to a cellphone via Bluetooth.
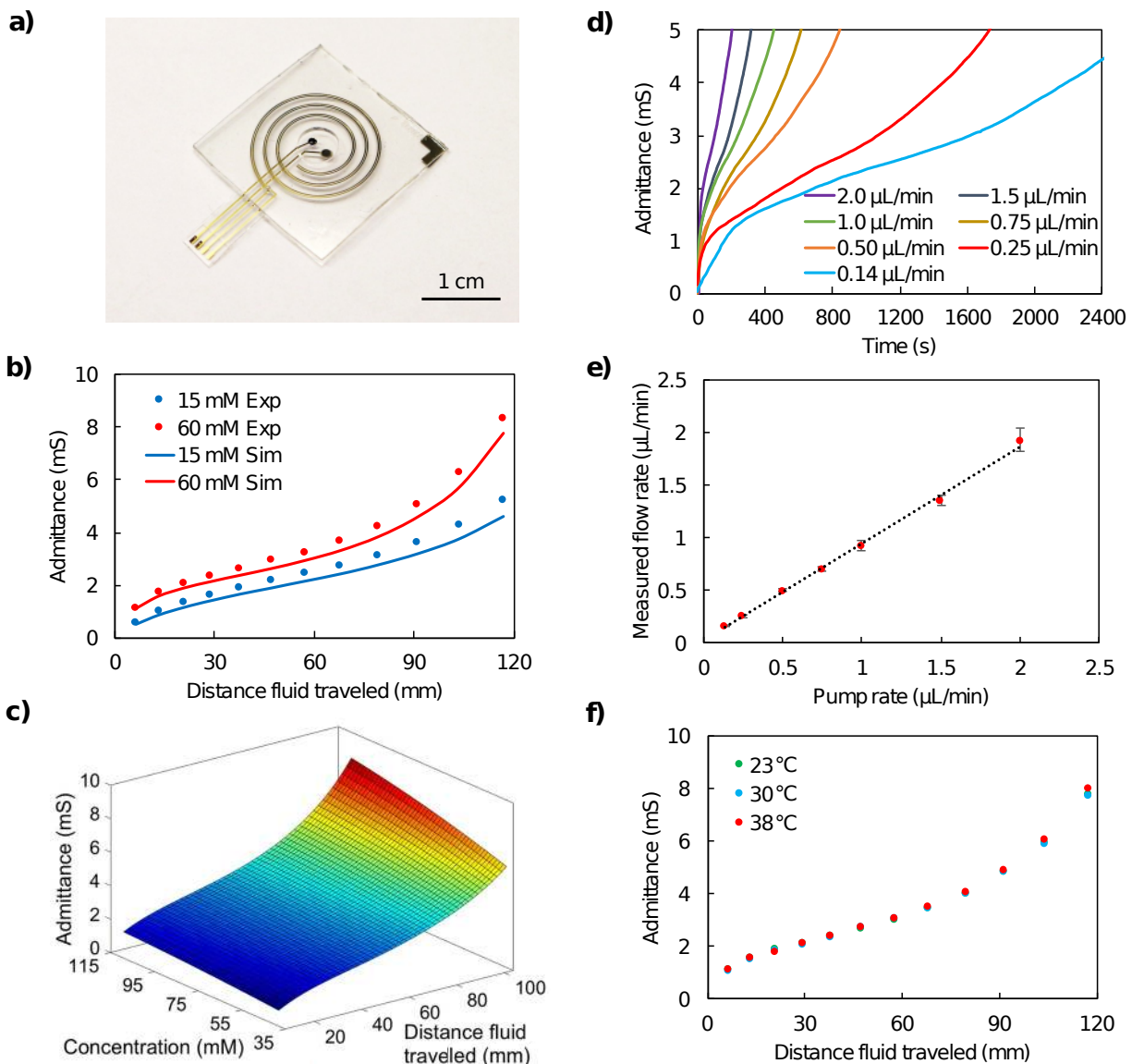
Figure 2. (a) An optical image of the sensing component of the sweat sensing patch. (b) Change in admittance along with the distance traveled by the fluid. Experimental and simulation results in 15 and 60 mM [Na⁺] are plotted. (c) A color map showing the relation between admittance, [Na⁺], and distance traveled by the fluid. The map is plotted based on experimental results. (d) Admittance measurement in a 30mM NaCl solution at various pump rates. (e) Relation between pump rate by the commercial flow meter

and flow rate measured and converted using the calibration plot in **c**. (f) Temperature influence on the admittance measurement in 60 mM [Na$^+$]. Each curve is obtained by averaging four repeated trials at each temperature as shown in Figure S4.
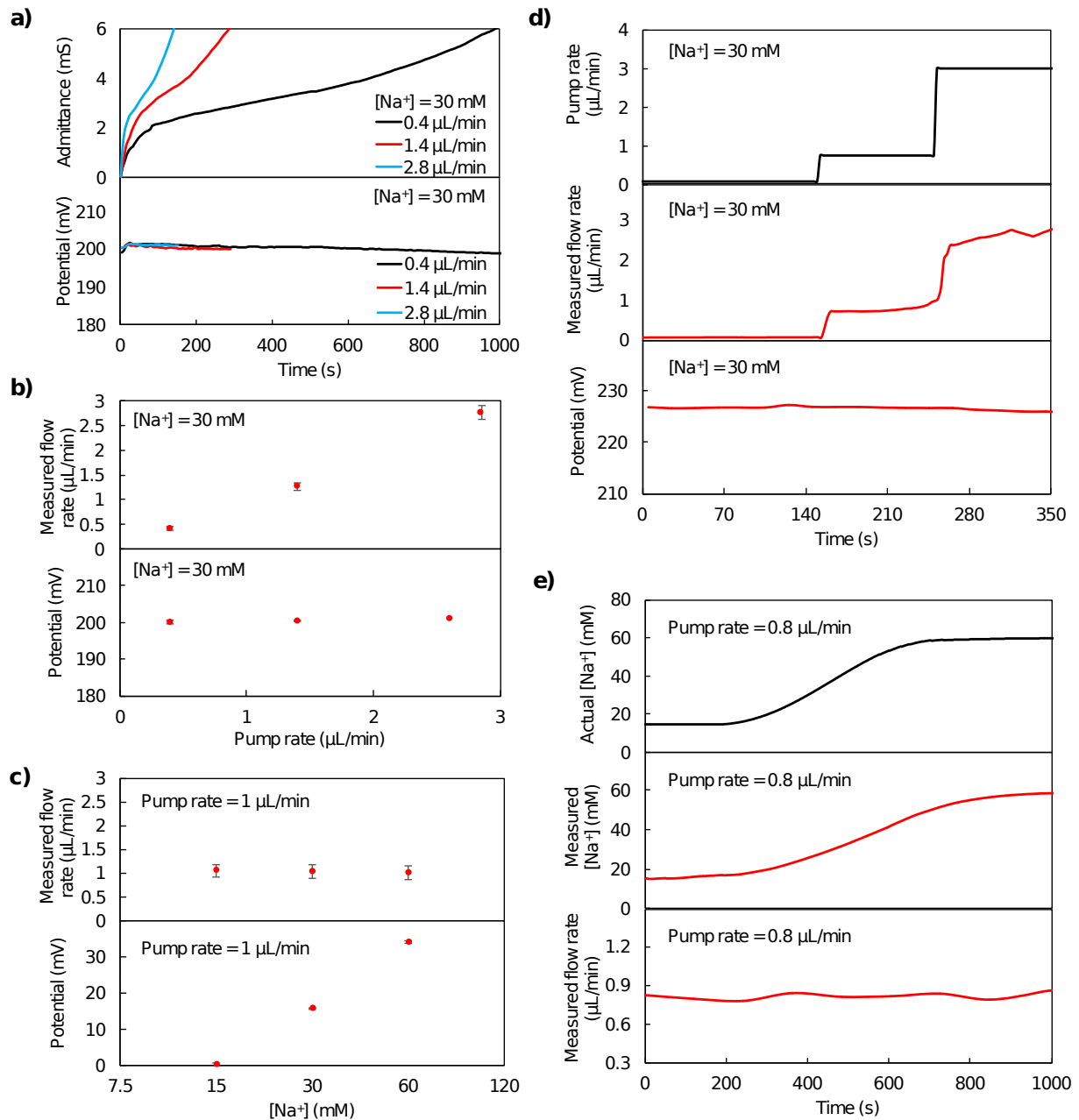
Figure 3. Off-body simultaneous measurement of [Na⁺] and flow rate. (a) Admittance and OCP measurement in 30 mM [Na⁺] and various pump rates. (b) Flow rate computed from admittance measurement and OCP in **a** vs pump rate in 30 mM [Na⁺]. (c) Flow rate and OCP measurements at a constant pump rate of 1 µL/min and varying [Na⁺]. The sensitivity of the Na⁺

sensor shown here is 56 mV/decade. (d) Flow rate and OCP measurements by performing a temporal change in pump rate using a commercial syringe pump meter and maintaining a constant [Na$^+$]. (e) [Na$^+$] and flow rate measurements at a constant pump rate and a temporal change in [Na$^+$].
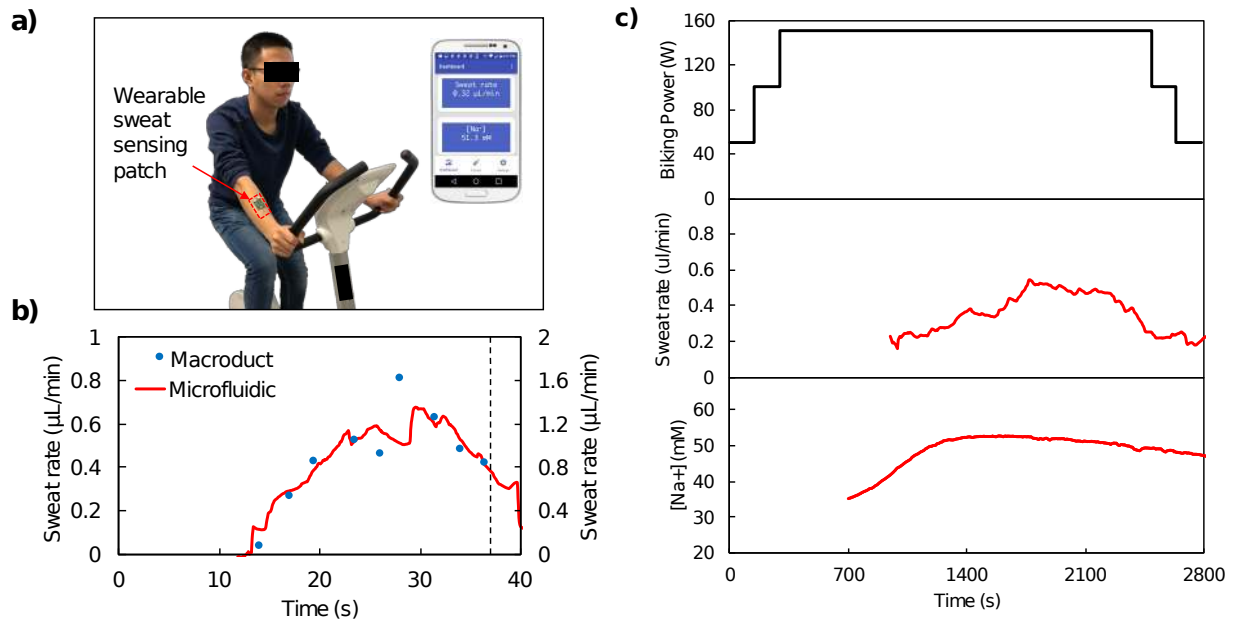
Figure 4. On-body analyses of sweat rate and [Na$^+$]. (a) An optical image of a subject wearing the sweat sensing patch. The data is wirelessly transmitted to a cellphone and is displayed in a customized cellphone app. (b) Comparison of electrical sweat rate measurement from the microfluidic sweat rate sensor and optical measurement using the Macroduct®. The dash line indicates the end of cycling. (c) On-body simultaneous measurements of sweat rate and [Na$^+$] using the sweat sensing patch at a constant biking power of 150 W.

ASSOCIATED CONTENT

Supplementary Information Available: The following files are available free of charge.

Supporting Information. Figure S1-S6 are referenced in the paper.

AUTHOR INFORMATION

Corresponding Author

*E-mail: ajavey@berkeley.edu

Author Contributions

H. Y. Y. N led the experiments with assistance from L. C. T. and Q. P. N. M. C. designed and built the PCB. G. Z. did the simulations. W. G., M. B., J. B., H. K., and H. M. F. provided assistance for the fabrications and the experimental procedures.

Notes

The authors declare no competing financial interest.

REFERENCES

(1) Schwartz, G.; Tee, B. C. K.; Mei, J.; Appleton, A. L.; Kim, D. H.; Wang, H.; Bao, Z. Flexible Polymer Transistors with High Pressure Sensitivity for Application in Electronic Skin and Health Monitoring. *Nat. Commun.* **2013,** *4,* 1859.

(2) Wang, C.; Hwang, D.; Yu, Z.; Takei, K.; Park, J.; Chen, T.; Ma, B.; Javey, A. User-Interactive Electronic Skin for Instantaneous Pressure Visualization. *Nat. Mater.* **2013,** *12,* 899−904.

(3) Kaltenbrunner, M.; Sekitani, T.; Reeder, J.; Yokota, T.; Kuribara, K.; Tokuhara, T.; Drack, M.; Schwodiauer, R.; Graz, I.; Bauer Gogonea, S.; Bauer, S.; Someya, T. An Ultra-Lightweight Design for Imperceptible Plastic Electronics. *Nature* **2013,** *499,* 458−463.

(4) Tee, B. C. K.; Chortos, A.; Berndt, A.; Nguyen, A. K.; Tom, A.; McGuire, A.; Lin, Z. C.; Tien, K.; Bae, W.; Wang, H.; Mei, P.; Chou, H.; Cui, B.; Deisseroth, K.; Ng, T. N.; Bao, Z. A Skin-Inspired Organic Digital Mechanoreceptor. *Science* **2015,** *350,* 313−316.

(5) Yamamoto, D.; Nakata, S.; Kanao, K.; Arie, T.; Akita.; Takei, K. A Planar, Multisensing Wearable Health Monitoring Device Integrated with

Acceleration, Temperature, and Electrocardiogram Sensors. *Adv. Mat. Tech.* **2017,** *2,* 1700057.

(6) Ota, H.; Chao, M.; Gao, Y.; Wu, E.; Tai, L.-C.; Chen, K.; Matsuoka, Y.; Iwai, K.; Fahad, H. M.; Gao, W.; Nyein, H. Y. Y.; Lin, L.; Javey, A. 3D Printed Earable Smart Devices for Real-time Detection of Core Body Temperature. *ACS Sens.* **2017,** *2,* 990-997.

(7) Gao, W.; Emaminejad, S.; Nyein, H. Y. Y.; Challa, S.; Chen, K.; Peck, A.; Fahad, H. M.; Ota, H.; Shiraki, H.; Kiriya, D.; Lien, D.-H.; Brooks, G. A.; Davis, R. W.; Javey, A. Fully Integrated Wearable Sensor Arrays for Multiplexed in Situ Perspiration Analysis. *Nature* **2016,** *529,* 509−514.

(8) Bandodkar, A. J.; Jeerapan, I.; Wang, J. Wearable Chemical Sensors: Present Challenges and Future Prospects. *ACS Sens.* **2016,** *1,* 464−482.

(9) Wang, S.; Chinnasamy, T.; Lifson, M. A.; Inci, F.; Demirci, U. Flexible Substrate-Based Devices for Point-of-Care Diagnostics. *Trends Biotechnol.* **2016,** *34,* 909-921.

(10) Xu, S.; Zhang, Y.; Jia, L.; Mathewson, K. E.; Jang, K.-I.; Kim, J.; Fu, H.; Huang, X.; Chava, P.; Wang, R.; Bhole, S.; Wang, L.; Na, Y. J.; Guan, Y.; Flavin, M.; Han, Z.; Huang, Y.; Rogers, J. A. Soft Microfluidic Assemblies of Sensors, Circuits, and Radios for the Skin. *Science* **2014,** *344,* 70−74.

(11) Gao, Y.; Ota, H.; Schaler, E. W.; Chen, K.; Zhao, A.; Gao, W.; Fahad, H. M.; Leng, Y.; Zheng, A.; Xiong, F.; Zhang, C.; Tai, L.-C.; Zhao, P.; Fearing, R. S.; Javey, A. Wearable Microfluidic Daiphragm Pressure Sensor for Health and Tactile Touch Monitoring. *Adv. Mater.* **2017,** *29,* 1701985.

(12) Lee, J. W.; Xu, R.; Lee, S.; Jang, K.-I.; Yang, Y.; Banks, A.; Yu, K. J.; Kim, J.; Xu, S.; Ma, S.; Jang, S. W.; Won, P.; Li, Y.; Kim, B. H.; Choe, J. Y.; Huh, S.; Kwon, Y. H.; Huang, Y.; Paik, U.; Rogers. J. A. Soft, thin skin-mounted power management systems and their use in wireless thermography. *PNAS* **2016,** *11,* 6131–6136.

(13) Li, X.; Dunn, J.; Salins, D.; Zhou, G.; Zhou, W.; Rose, S. M. S.-F., Perelman, D.; Colbert, E.; Runge, R.; Rego, S.; Sonecha, R.; Datta, S.; MaLaughlin, T.; Snyder, M. Digital Health: Tracking Physiomes and Activity Using Wearable Biosensors Reveals Useful Health-Related Information. *PLOS Biol.* **2017,** *15,* e2001402.

(14) Schazmann, B.; Morris, D.; Slater, C.; Beirne, S.; Fay, C.; Reuveny, R.; Moyna, N.; Diamond, D. A wearable electrochemical sensor for the real-time measurement of sweat sodium concentration. *Anal. Methods* **2010**, *2*, 342-348.

(15) Kim, J.; Jeerapan, I.; Imani, S.; Cho, T. N.; Bandodkar, A.; Cinti, S.; Mercier, P. P.; Wang, J. Noninvasive Alcohol Monitoring Using a Wearable Tattoo-Based Iontophoretic-Biosensing System. *ACS Sens.* **2016,** *1,* 1011–1019.

(16) Gao, W.; Nyein, H. Y. Y.; Zhahpar, Z.; Fahad, H. M.; Chen, K.; Emaminejad, S.; Gao, Y.; Tai, L.-C.; Ota, H.; Wu, E.; Bullock, J.; Zeng, Y.; Lien, D.-H.; Javey, A. Wearable Microsensor Array for Multiplexed Heavy Metal Monitoring of Body Fluids. *ACS Sens.* **2016,** *1,* 866–874.

(17) Rose, D. P.; Ratterman, M. E.; Griffin, D. K.; Hou, L.; Keely-Loughnane,

N.; Naik, R. R.; Hagen, J. A.; Papautsky, I.; Heikenfeld, J. C. Adhesive RFID Sensor Patch for Monitoring of Sweat Electrolytes. *IEEE Trans. Biomed. Eng.* **2015,** *62,* 1457–1465.

(18) Anastasova, S.; Crewther, B.; Bembnowicz, P.; Curto, V.; Ip, H. M.; Yang, G. Z. A wearable multisensing patch for continuous sweat monitoring. *Biosens. Bioelectron.* **2017,** *93,* 139–145.

(19) Kinnamon, D.; Ghanta, R.; Lin, K.-C.; Muthukumar, S.; Prasad, S. Portable biosensor for monitoring cortisol in low-volume perspired human sweat. *Sci. Rep.* **2017,** DOI:10.1038/s41598-017-13684-7.

(20) Heikenfeld, J. Non-Invasive Analyte Access and Sensing through Eccrine Sweat: Challenges and Outlook circa. *Electroanalysis* **2016,** *28,* 1242−1249.

(21) Sonner, Z.; Wilder, E.; Heikenfeld, J.; Kasting, G.; Beyette, F.; Swaile, D.; Sherman, F.; Joyce, J.; Hagen, J.; Kelley-Loughnane, N.; Naik, R. The Microfluidics of the Eccrine Sweat Gland, Including Biomarker Partitioning, Transport, and Biosensing Implications. *Biomicrofluidics* **2015,** *9,* 031301.

(22) N, D. G. N. and F. The current status of sweat testing for drugs of abuse: a review. *Curr Med Chem*. **2013,** *20,* 545-61.

(23) Nyein, H. Y. Y.; Gao, W.; Shahpar, Z.; Emaminejad, S.; Challa, S.; Chen, K.; Fahad, H. M.; Tai, L.-C.; Ota, H.; Davis, R. W.; Javey, A. A Wearable Electrochemical Platform for Noninvasive Simultaneous Monitoring of Ca2+ and Ph. *ACS Nano* **2016,** *10,* 7216−7224.

(24) Emaminejad, S.; Gao, W.; Wu, E.; Davies, Z. A.; Yin Yin Nyein, H.; Challa, S.; Ryan, S. P.; Fahad, H. M.; Chen, K.; Shahpar, Z.; Talebi, S.; Milla, C.; Javey,

A.; Davis, R. W. Autonomous Sweat Extraction and Analysis Applied to Cystic Fibrosis and Glucose Monitoring Using a Fully Integrated Wearable Platform. *PNAS* **2017,** *114,* 4625−4630.

(25) Emrich, H. M.; Stoll, E.; Friolet, B.; Colombo, J. P.; Richterich, R.; Rossi, E. Sweat Composition in Relation to Rate of Sweating in Patients with Cystic Fibrosis of the Pancreas. *Pediat. Res.* **1968,** *2,* 464-478.

(26) Sakharov, D. A.; Shkurnikov, M. U.; Vagin, M. Y.; Yashina, E. I., Karyakin, A. A.; Tonevitsky, A. G. Relationship between Lactate Concentrations in Active Muscle Sweat and Whole Blood. *Bull Exp Biol Med.* **2010,** *150,* 83-85.

(27) Driskell, J. A.; Wolinsky, I. Nutritional Assessment of Athletes, Second Edition. CRC Press, 2016. 354-359.

(28) Shirreffs, S. M.; Maughan, R. J. Whole body sweat collection in humans: an improved method with preliminary data on electrolyte content. *J. Appl. Physiol.* **1997,** *82,* 336-341.

(29) Buono, M. J.; Ball, K. D.; Kolkhorst, F. W. Sodium ion concentration vs. sweat rate relationship in humans. *J Appl. Physiol* **2007,** *103,* 990-994.

(30) Baker, L. B.; Stofan, J. R.; Lukaski, H. C.; Horswill, C. A. Exercise-Induced Trace Mineral Element Concentration in Regional Versus Whole-Body Wash-Down Sweat. *Int. J. Sport Nutr. Exerc. Metab.* **2011,** *21,* 233-239.

(31) Salvo, P.; Francesco, F. D.; Costanzo, D.; Ferrari, C.; Trivella, M. G.; Rossi, D. D. A Wearable Sensor for Measuring Sweat Rate. *IEEE Sens. J.* **2010,** *10,* 1557-1558.

(32) Coyle, S.; Morris, D.; Lau, K. T.; Diamond, D.; Taccini, N.; Costanzo, D.; Salvo, P.; Francesco, F. D.l Trivella, M. G.; Porchet, J. A.; Luprano, J. Textile sensors to measure sweat pH and sweat-rate during exercise. Pervasive Computing Technologies for Healthcare, 2009. PervasiveHealth 2009. 3rd International Conference.

(33) Koh, A.; Kang, D.; Xue, Y.; Lee, S.; Pielak, R. M.; Kim, J.; Hwang, T.; Min, S.; Banks, A.; Bastien, P.; Manco, M. C.; Wang, L.; Ammann, K. R.; Jang, K.-I.; Won, P.; Han, S.; Ghaffari, R.; Paik, U.; Slepian, M. J.; Balooch, G.; Huang, Y.; Rogers, J. A. A Soft, Wearable Microfluidic Device for the Capture, Storage, and Colorimetric Sensing of Sweat. *Sci. Transl. Med.* **2016,** *8,* 366ra165.

(34) Martín, A.; Kim, J.; Kurniawan, J. F.; Sempionatto, J. R.; Moreto, J. R.; Tang, G.; Campbell, A. S.; Shin, A.; Lee, M. Y.; Liu, X.; Wang, J. Epidermal Microfluidic Electrochemical Detection System: Enhanced Sweat Sampling and Metabolite Detection. *ACS Sens.* **2017,** DOI: 10.1021/acssensors.7b00729.

(35) Tang, L.; Lee, N. Y. A facile route for irreversible bonding of plastic-PDMS hybrid microdevices at room temperature. *Lab Chip* **2010,** *10*, 1274-1280.

(36) Todnem, L.; Knudsen, G.; Riise, T.; Nyland, H.; Aarli, J. A. The non-inear relationship between nerver conduction velocity and skin temperature. *J. Neurol. Neurosurg. Psychiatry* **1989,** *52,* 497-501.

(37) Rica, R, A.; Bazant, M. Z. Electrodiffusiophoresis: Particle motion in electrolytes under direct current. *Phys. Fluids* **2010,** *22,* 112109.

(38) Hammond, K. B.; Turcios, N. L.; Gibson, L. E. Clinical evaluation of the macroduct sweat collection system and conductivity analyzer in the diagnosis of cystic fibrosis. *The J. of Pediatrics* **1994,** *124,* 255-260.

(39) Habibi, M.; Klemer, D. P.; Raicu, V. Two-dimensional dielectric spectroscopy: Implementation and validation of a scanning open-ended coaxial probe. *Rev. Sci. Instrum*. **2010,** *81,* 075108.

(40) Renou, R.; Ding, M.; Zhu, H.; Szymczyk, A.; Malfreyt, P.; Ghoufi, A. Concentration dependence of the dielectric permittivity, structure, and dynamics of aqueous NaCl solutions: Comparison between the drude oscillator and electronic continuum models. *J. Phys. Chem. B.* **2014,** *118,* 3931-3940.

(41) Gavish, N.; Promislow, K. Dependence of the dielectric constant of electrolyte solutions on ionic concentration: A microfield approach. *Phys. Rev. E.* **2016,** *94,* 012611.

(42) Lima, L. F.; Vieria, A. L.; Mukai, H.; Andrade, C. M. G.; Fernandes, P. R. G. Electric impedance of aqueous KCl and NaCl solutions: Salt concentration dependence on components of the equivalent electric circuit. *J. Mol. Liq.* **2017,** *241,* 530-539.

For TOC only: